Computational Fluid Dynamics JOURNAL vol.2 no.3 October 1993 (319 — 338)

NUMERICAL ANALYSIS OF FULLY DEVELOPED TURBULENT FLOW IN A SQUARE DUCT WITH TWO FACING ROUGHENED WALLS

Hitoshi SUGIYAMA†
Mitsunobu AKIYAMA† Masashi MATSUMOTO†
Masaru HIRATA‡ Nao NINOMIYA†

Abstract

A numerical analysis has been performed for fully developed turbulent flow in a square duct with two roughened facing walls by using newly developed algebraic stress model. The calculated results were compared with experimental data and and validation of this method is confirmed. In a square duct with smooth walls, as is well known, a pair of vortices is observed in a quadrant of the duct cross section. In this rough duct, however, both results by the present method and the experiment revealed formation of only one vortex in a quadrant. The calculated distributions of the normal stresses and the turbulent energy are in reasonably good agreement with the experimental data. Moreover, vorticity balance is examined by evaluating production term in the vorticity transport equation using the calculated results of the two cases of a square duct with smooth walls and with two roughened walls. As a result of this examination, it was found that the distribution of the production term generated by the normal stresses is similar to the one of the shear stress with opposite sign in both duct cases.

1. INTRODUCTION

Since heat transfer surfaces are often roughened to enhance the convective heat transfer by promoting turbulence, ducts with non-circular cross section with roughened walls are often encountered in engineering practice. The flows in such duct are accompanied by the secondary flow of the second kind which is induced by anisotropic turbulence, and the distributions of Reynolds stresses in such cases are influenced by the roughened walls. Although this secondary velocity is only of two or three percent of the streamwise bulk velocity, its presences displaces the lines of constant axial velocity considerably toward the corners of the duct, yielding a relatively high velocity field there. Furthermore the secondary motion produces an increase of the wall shear stress towards the corners. Therefore, understanding of the characteristics of the secondary flow in a non-circular duct with rough walls is indispensable for clarifying the effects of rough walls on turbulent convective heat transfer.

Presented at the 6th Numerical Fluid Dynamics Symposium at Tokyo on Dec. 21 – 23, 1992.
Received on February 17, 1993. Revised on July 13, 1993.

† Dept. Mechanical Systems Engineering, Utsunomiya University; Ishii-cho 2753, Utsunomiya 321, Japan
‡ Dept. Mechanical Engineering, Shibaura Institute of Technology; Fukasaku 307, Oomiya 330, Japan

In experimental analysis, Launder and Ying [1] have carried out the measurement of the secondary flow in a duct with equally roughened surfaces. Fujita *et al.* have measured the distributions of Reynolds stresses and the flow pattern of secondary flow in detail for a square duct with two roughened facing walls [2] and for the one with a roughened wall [3]. Although the surface condition is different from the experiment of [3], Humphrey and Whitelaw [4] also have measured the Reynolds stresses in a square duct with a roughened wall. Recently, the experimental results about a mean temperature field obtained in forced convection heat transfer for a turbulent flow through a square duct with a rough wall have been presented by Hirota *et al.* [5]. Furthermore, they have examined the mechanism of the heat transfer enhancement by the rough wall based on the transport equations of Reynolds stress and turbulent heat flux.

On the other hand, in numerical analysis, Hanjalic and Launder [6] have calculated the asymmetric flow introduced by fixing ribs of square cross-section aligned normal to the flow and pitched 10 rib heights apart to one wall. However, their numerical analysis has been carried out for two dimensional turbulent flow without accounting the secondary flow of the second kind. Demuren and Rodi [7] calculated the fully developed turbulent flow in a 5:1 ratio rectangular channel with a roughened wall, which was also studied experimentally by Hinze [8]. The calculation results revealed the distortion of the primary velocity contours, and the distributions of the turbulent shear stress and the kinetic energy along the wall bisector were presented. Fujita *et al.* [9] performed a flow calculation in a square duct with two roughened facing walls using $k-\varepsilon$ model coupled with the algebraic stress model developed by Launder and Ying [10]. Though they obtained the velocity vectors of the secondary flow, the calculated flow pattern was considerably different from the experimental data of [2].

Sugiyama *et al.* [11] have made comparative study of several typical Reynolds stress models and, based on these examinations, presented an improved pressure strain correlations of the Reynolds stress equations, which is used in the present study. Very few calculations about non-circular ducts with rough walls have been reported, which discussed about the influence of rough walls on the secondary flow behavior and on the mechanism of the secondary flow generation. Therefore, the first purpose of the present research is to analyze the developed turbulent flow in a square duct with two roughened facing walls, which was experimentally studied in [2], and to validate this Reynolds stress model. The second purpose is to evaluate the production term in the vorticity transport equation using the calculated results in order to make the generation mechanism of the secondary flow clear.

2. TECHNIQUE OF ANALYSIS

2.1 Subject of Numerical Analysis

As the subject of numerical analysis, we have adopted the experimental data for the fully developed turbulent flow in a square duct with two roughened facing walls presented in [2]. Figure 1 shows the orthogonal coordinate system set in duct and a schematic diagram of the experimental apparatus. The duct has a 50 mm square cross section and is 4500 mm in length. Roughness element whose cross-section was 1 mm square were located at 10 mm intervals, transverse to the primary flow, to make up the two roughened facing walls of the duct. Reynolds number Re, defined as $U_b D_h/\nu$, where U_b is the bulk velocity, D_h is the hydraulic diameter and ν is the

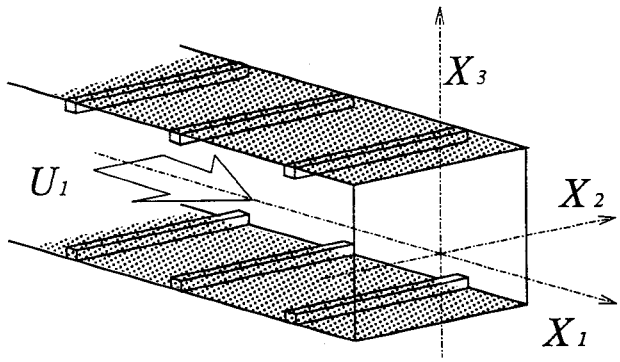

Fig.1: Subject of calculation and coordinate system

kinematic viscosity of air, was set to be 6.5×10^4. Measurement were conducted at the cross section of 10 mm upstream from the duct exit by using a hot wire anemometer. This measuring cross section is equal to the location of $89.8\,D_h$, which is considered in the fully developed region.

2.2 Reynolds Stress Model

The anisotropy nature of the turbulence is expressed by the Reynolds stress equations. A set of the differential equations governing the transport of the Reynolds stresses are derived from the Navier-Stokes equation, namely:

$$\frac{\mathrm{D}\overline{u_iu_j}}{\mathrm{D}t} = -\left(\overline{u_iu_k}\frac{\partial U_j}{\partial x_k} + \overline{u_ju_k}\frac{\partial U_i}{\partial x_k}\right) + \overline{\frac{p}{\rho}\left(\frac{\partial u_i}{\partial x_j} + \frac{\partial u_j}{\partial x_i}\right)}$$
$$- \frac{\partial}{\partial x_k}\left[\overline{u_iu_ju_k} - \nu\frac{\partial \overline{u_iu_j}}{\partial x_k} - \overline{\frac{p}{\rho}\left(\delta_{jk}u_i + \delta_{ik}u_j\right)}\right] - 2\nu\overline{\frac{\partial u_i}{\partial x_k}\frac{\partial u_j}{\partial x_k}}. \qquad (1)$$

The first term of right hand side is the production term P_{ij}, the second term is the pressure strain correlation π_{ij}, the third term is the diffusion term, and the fourth term is the dissipation term ε_{ij}. The solution of the Reynolds stress equation in the above form (1) is difficult to obtain, and model assumptions for these terms are introduced. The convective and diffusion terms, using Rodi's approximation [12], are transformed into the algebraic form. Following Chou [13], the pressure-strain term are expressed as follows:

$$\overline{\frac{p}{\rho}\frac{\partial u_i}{\partial x_j}} = \frac{1}{4\pi}\int_{\mathrm{vol}}\left\{\overline{\left(\frac{\partial^2 u_l u_m}{\partial x_l \partial x_m}\right)'\frac{\partial u_i}{\partial x_j}} + 2\left(\frac{\partial U_l}{\partial x_m}\right)'\overline{\left(\frac{\partial x_m}{\partial x_l}\right)'\left(\frac{\partial u_i}{\partial x_j}\right)}\right\}\frac{\mathrm{d\,VOL}}{|\boldsymbol{x}-\boldsymbol{y}|} + S_{ij} \qquad (2)$$

where the terms with and without the prime correspond to the values at y and x, respectively. The first and second terms of the right hand side of (2) are relevant to the interaction of the fluctuating velocities and to the one of the mean strain and fluctuating velocities, respectively. The term S_{ij} represents the wall effect. In the present model, the Rotta's linear return-to-

isotropy model is applied to the first term, which is:

$$(\pi_{ij,1} + \pi_{ji,1}) = -c_1 \frac{\varepsilon}{k} \left(\overline{u_i u_j} - \frac{2}{3}\delta_{ij} k \right) \tag{3}$$

where k and ε are the time-averaged, turbulence kinetic energy and the energy dissipation rate, respectively, and c_1 represents an empirical constant.

For $\pi_{ij,2}$ the correlation is approximated in the form:

$$\pi_{ij,2} = \left(\frac{\partial U_l}{\partial x_m} \right) a_{lj}^{mi} \tag{4}$$

where a_{lj}^{mi} is the forth-order tensor, which is determined by the following kinematic constraints:

$$a_{lj}^{mi} = a_{lj}^{im} = a_{jl}^{im} \tag{5}$$

$$a_{li}^{mi} \frac{\partial U_l}{\partial x_m} = 0 \tag{6}$$

$$a_{jj}^{mi} = 2\overline{u_m u_i}. \tag{7}$$

The constraint (6) is different from Rotta's proposal, and is chosen for the reason that $\pi_{ij,2}$ is defined as the product between the fourth order tensor and the mean strain as seen in (4). The constraints in the form of (5), (6) and (7) arise from symmetry, mass conservation and Green's theorem, respectively. The form of (7) suggests that the fourth-order tensor might be approximated by linear combination of the Reynolds stresses. The most general such tensor satisfying the symmetry constraints implied by (7) is written as:

$$\begin{aligned} a_{lj}^{mi} = {} & \alpha \delta_{lj} \overline{u_m u_i} + \beta \left(\delta_{ml} \overline{u_i u_j} + \delta_{mj} \overline{u_i u_l} + \delta_{il} \overline{u_m u_j} + \delta_{ij} \overline{u_m u_l} \right) \\ & + c_2 \delta_{mi} \overline{u_l u_j} + \left\{ \eta \delta_{mi} \delta_{lj} + \nu \left(\delta_{ml} \delta_{ij} + \delta_{mj} \delta_{il} \right) \right\} k \end{aligned} \tag{8}$$

which is proposed by Launder *et al.* [14]. The symbol δ_{ij} represents the Kronecker delta and c_2, α, β, η, ν are empirical constants. The application of (6) and (7) enables two constants of (8) to be expressed in terms of c_2. On combining (4) and (8), the complete influence of the mean strain on the pressure-strain correlation is expressed in the following form:

$$\left.\begin{aligned} (\pi_{ij,2} + \pi_{ji,2}) = {} & -(\alpha + \beta) \left(P_{ij} - \frac{2}{3} P_k \delta_{ij} \right) + \zeta \left(\frac{\partial U_i}{\partial x_j} + \frac{\partial U_j}{\partial x_i} \right) k \\ & + (4\beta + \alpha)(D_{ij} - \frac{2}{3} P_k \delta_{ij}) \\ D_{ij} = {} & -\overline{u_i u_k} \frac{\partial U_k}{\partial x_j} - \overline{u_j u_k} \frac{\partial U_k}{\partial x_i} \\ \alpha = {} & \frac{1}{11}(4c_2 + 10) \quad \beta = -\frac{1}{11}(2 + 3c_2) \quad \zeta = \eta + \nu. \end{aligned}\right\} \tag{9}$$

In the above equation, ζ is the independent constant to be determined from experimental data and α and β are defined as the functions of c_2. On the other hand, in the model of [12],

Table 1: Modeling of the pressure-strain correlation term

$\pi_{ij,1}+\pi_{ji,1}$	$-c_1\frac{\varepsilon}{k}\left(\overline{u_iu_j}-\frac{2}{3}k\delta_{ij}\right)$
$\pi_{ij,2}+\pi_{ji,2}$	$-\frac{c_2+8}{11}\left(P_{ij}-\frac{2}{3}P_k\delta_{ij}\right)+\zeta k\left(\frac{\partial U_i}{\partial x_j}+\frac{\partial U_j}{\partial x_i}\right)-\frac{8c_2-2}{11}\left(D_{ij}-\frac{2}{3}P_k\delta_{ij}\right)$
$[\pi_{ij}+\pi_{ji}]_w$	$c_1=c_1^*+c_1'f\left(\frac{L}{X_w}\right),\quad c_2=c_2^*+c_2'f\left(\frac{L}{X_w}\right),\quad \zeta=\zeta^*+\zeta'f\left(\frac{L}{X_w}\right)$

$$P_{ij}=-\overline{u_iu_k}\frac{\partial U_j}{\partial x_k}-\overline{u_ju_k}\frac{\partial U_i}{\partial x_k}\qquad D_{ij}=-\overline{u_iu_k}\frac{\partial U_k}{\partial x_j}-\overline{u_ju_k}\frac{\partial U_k}{\partial x_i}$$

ζ, α and β are defined as the functions of c_2 only. Therefore, in the present model, we can take into account more experimental data than that model does [14].

The wall effect term $\pi_{ij,w}$ on the turbulent stresses is counted in this model by making the empirical constants as functions of the dimensionless distance L/X_w from the wall:

$$\left.\begin{aligned}c_1&=c_1^*+c_1'f(L/X_w)\\c_2&=c_2^*+c_2'f(L/X_w)\\\zeta&=\zeta^*+\zeta'f(L/X_w)\end{aligned}\right\},\tag{10}$$

$$f(\frac{L}{X_w})=\frac{C_\mu^{3/4}k^{3/2}}{\kappa\varepsilon}\frac{1}{X_w}\tag{11}$$

where X_w expresses the distance from the wall and L is defined by the length scale of turbulence, and C_μ and κ represent the empirical and the von Karman constant, respectively. The function $f(L/X_w)$ expresses the influence of the wall and takes a value of 1 in its vicinity, approaching to 0 with the increase of the distance. This value has been chosen such that, when $f=0$, the model yields the correct Reynolds stress components for nearly homogeneous shear flow by Champagne *et al.* [15], and, when $f=1$, the relative magnitude of the stress components agrees with the common value of near wall turbulence. Moreover, the experimental data of Harris *et al.* [16] which reported further homogeneous shear flow data where the strain rate is higher than the one in [15]. The pressure-strain correlation terms and constants used in this analysis are summarized in the Tables 1 and 2, respectively.

The fourth term of (1) is the homogeneous part of dissipation, which is commonly modeled under the assumption of the isotropic motion for the dissipation, namely:

$$\varepsilon_{ij}=2\nu\overline{\frac{\partial u_i}{\partial x_k}\frac{\partial u_j}{\partial x_k}}=\frac{2}{3}\delta_{ij}\varepsilon\tag{12}$$

Table 2: Constants in the pressure-strain correlation term

c_1^*	c_2^*	ζ^*	c_1'	c_2'	ζ'
1.4	0.44	−0.16	−0.35	0.12	−0.1

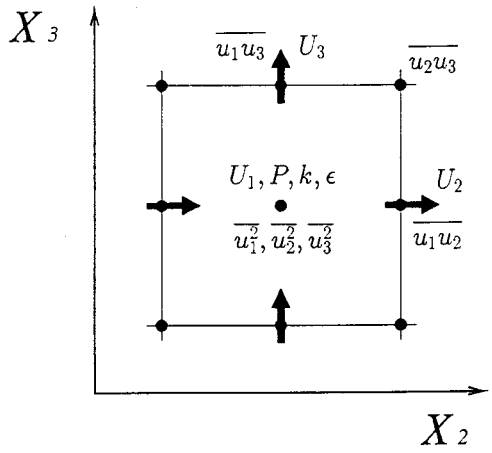

Fig.2: Locations of calculation parameters

2.3 Method of Numerical Analysis

Control volume method was applied using a uniform, staggered grid mesh, in which the locations of Reynolds stresses, vector and scaler parameters are defined as shown in Fig.2. In order to discretize the convection terms, the quadratic interpolation (QUICK) scheme is used for the momentum equations and the power law interpolation (PLDS) is for the transport equations of turbulent energy and turbulent dissipation. The SIMPLE (semi-implicit method for pressure linked equation) algorithm is used to solve the pressure equation and to have velocity correction. Computation was performed on a 20×20 uniform mesh over the quadrant of the duct for a Reynolds number of 6.5×10^4. Tests with various sizes of grids revealed that the solutions obtained are substantially grid-independent for mesh numbers of about 225 and greater.

The universal law of the wall and the local equilibrium condition applicable in the near wall region are utilized as the boundary conditions for the turbulent energy and dissipation. As the boundary condition on the roughened wall, the following empirical equation, proposed in [9] is applied:

$$\frac{U_l}{U_\tau} = \frac{1}{0.42}\ln\left(\frac{U_\tau y}{\nu}\right) - 8.4 \tag{13}$$

where U_τ represents the friction velocity. For the turbulent energy and dissipation, the above universal law for the rough wall is adopted as the boundary condition.

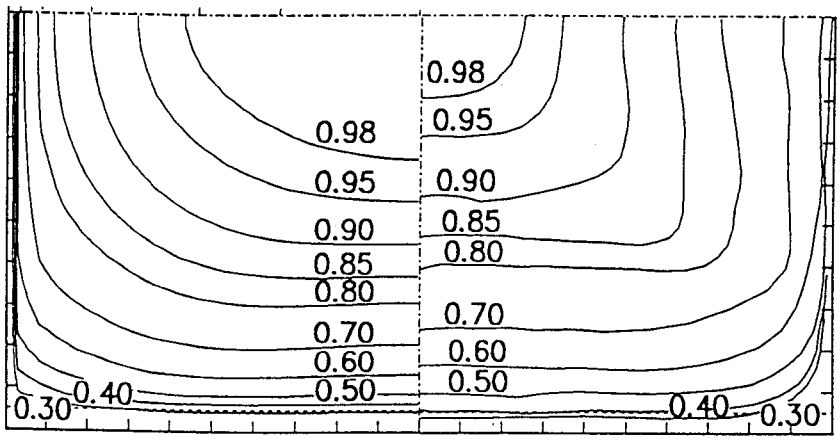

(a) Present calculation (b) Experiment by Fujita *et al.* [2]

Fig.3: Comparison of mean flow velocity U_1/U_s

3. ANALYSIS RESULTS AND CONSIDERATIONS

3.1 Comparison of Time Averaged Velocity

The contour maps of the mean velocity of the experimental results by Fujita *et al.* [2] and the present results are shown in Fig.3. The velocities are nondimensionalized by the axial mean flow velocity U_S at the duct center line. The dotted lines in it represent the height of the roughness elements. Although the bulging contours of the mean velocity towards the corner along the corner bisector are commonly observed in a square duct with smooth walls, such behavior is not found in this case. The experimental results shows a profile which is parallel to the rough wall. The present method is also able to predict this special feature.

Figure 4 displays the vector diagram of the secondary flow of the second kind for each result. All of them showed formations of only one longitudinal vortex in a quadrant, as seen in Fig.3 also.

Large discrepancy of the secondary flow pattern near the wall region of roughened face between the experimental and numerical results is observed in this figure. Concerning to these, reference [2] has pointed out that, although the measuring cross section is considered as in a fully developed flow, the flow near the roughness element is locally disturbed due to existence of the roughness elements, and as a result, large secondary flow is observed. Since numerical calculation has assumed that the wall surface has uniform roughness without localized roughness element, the numerical results do not indicate large secondary flow near the roughened wall. Except this discrepancy near the rough wall, both of the present numerical and the experimental results display the relatively large secondary flow along the smooth wall.

3.2 Comparison of Fluctuating Velocity

Figure 5 shows the turbulent energy obtained for each case, which has the maximum value near the rough wall and decreases toward the central region of the duct, and which are in good

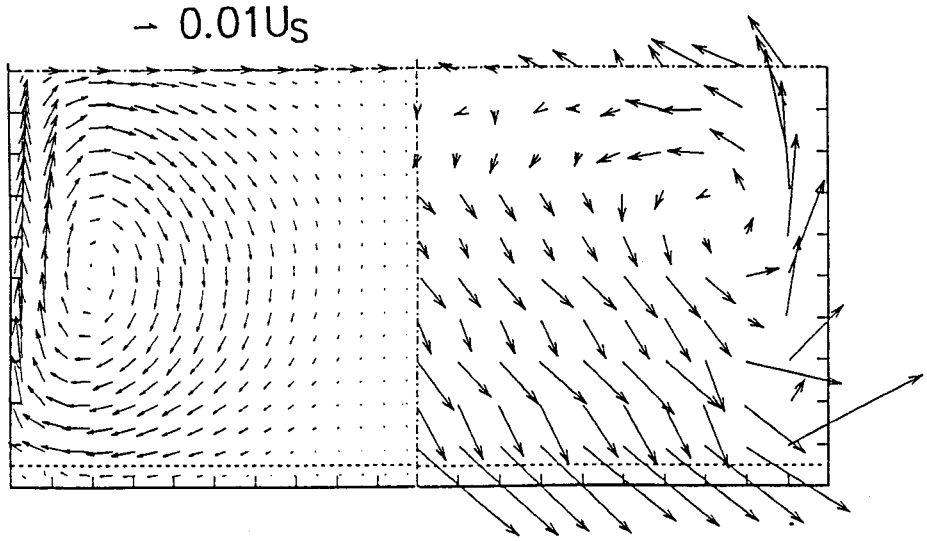

(a) Present calculation (b) Experiment by Fujita *et al.* [2]

Fig.4: Comparison of vector diagram of the secondary flow

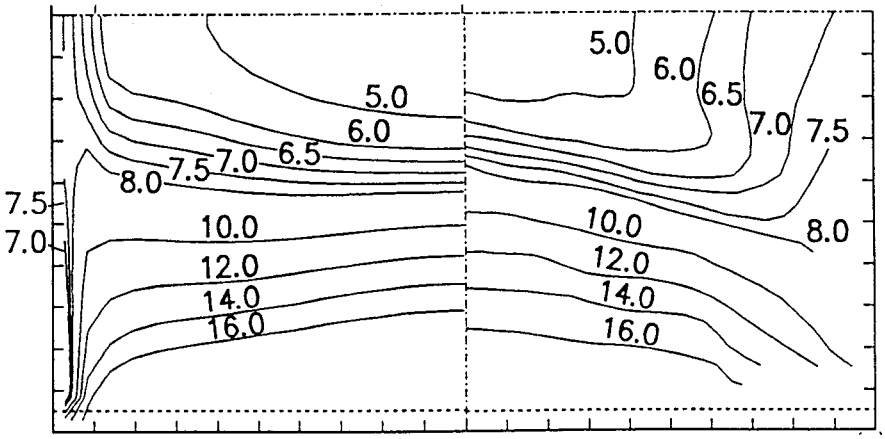

(a) Present calculation (b) Experiment by Fujita *et al.* [2]

Fig.5: Comparison of turbulent energy $k/U_s^2 \times 10^3$

agreements each other. The contour maps of these cases are different from those of a smooth duct which indicate bulging contours toward the corner region along the corner bisector.

Figure 6 shows the contour lines of the shear stress $\overline{u_1 u_2}$. In both of the present and the experimental results, the flowfield is divided into two regions with the opposite sign. In the present method, neglecting the derivative terms involving the secondary velocity, the equation

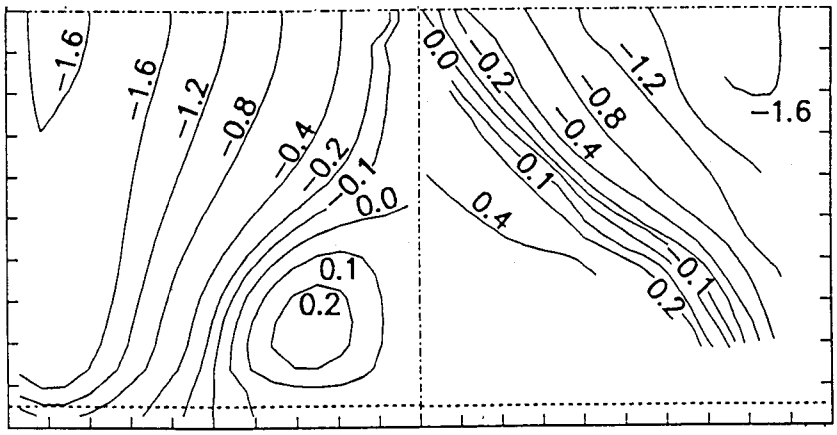

(a) Present calculation (b) Experiment by Fujita *et al.* [2]

Fig.6: Comparison of shear stress $\overline{u_1u_2}/U_s^2 \times 10^3$

of shear stress $\overline{u_1u_2}$ is expressed as follows:

$$-\overline{u_1u_2}\left\{\frac{P_k}{\varepsilon}-c_1+\frac{k}{\varepsilon}(1+3\beta)\frac{\partial U_1}{\partial X_1}\right\}=$$

$$\left\{\frac{k}{\varepsilon}(1-\alpha-\beta)\overline{u_2^2}+\frac{k}{\varepsilon}(4\beta+\alpha)\overline{u_1^2}+\frac{\zeta k^2}{\varepsilon}\right\}\frac{\partial U_1}{\partial X_2}. \tag{14}$$

On the other hand, in the case of [3], it is defined as follows:

$$-\overline{u_1u_2}=\nu_t\frac{\partial U_1}{\partial X_2} \tag{15}$$

where ν_t represents the isotropic eddy viscosity. Therefore, the signature change of the shear stress term $\overline{u_1u_2}$ is generated due to the change of the velocity gradient $\partial U_1/\partial X_2$. In other words, the signature changing is caused by the bulging contours of the mean flow velocity near the wall bisector which is caused by the secondary flow of the second kind. As seen in Fig.3, the experiment yields the contour lines which are parallel to the rough wall. This behavior is caused by the secondary flow of the second kind.

Figure 7 shows the contour lines of the shear stress $\overline{u_1u_3}$. The experimental data have the maximum value near the rough wall and a positive sign region of it appears near the center location along the smooth wall. This positive sign region is induced by changing of the derivative of the mean flow velocity with respect to X_3 direction as well as shear stress $\overline{u_1u_2}$. This discrepancy between the experimental and numerical results are caused by underestimating the secondary flow. Therefore, in order to predict this phenomenon, it is necessary to calculate the secondary flow preciously by modifying the turbulent model. Except this small discrepancy, the present method can predict the shear stress without much error.

Figure 8 shows the normal stress distributions $\overline{u_1^2}$, which are similar to those of the turbulent

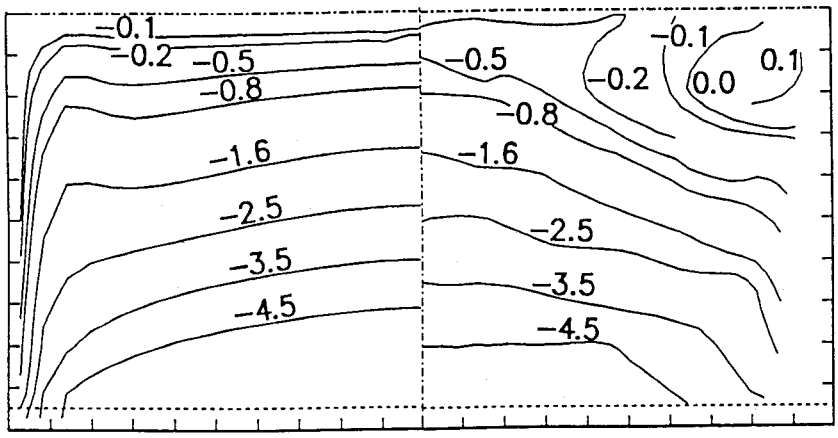

(a) Present calculation (b) Experiment by Fujita *et al.* [2]

Fig.7: Comparison of shear stress $\overline{u_1 u_3}/U_s^2 \times 10^3$

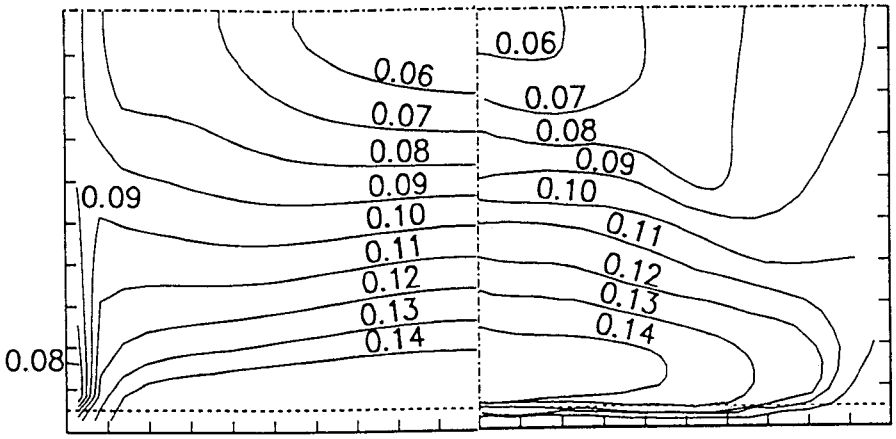

(a) Present calculation (b) Experiment by Fujita *et al.* [2]

Fig.8 Comparison of normal stress $\sqrt{\overline{u_1^2}}/U_s$

energy. The present calculation displays a good agreement with the experimental data near the rough wall and in the central regions.

Figure 9 shows the normal stress $\overline{u_2^2}$ which is the fluctuating velocity paralleled to rough wall. The maximum value of it appears near the rough wall and the small local minimum appear near the smooth walls and also the center of the section.

Figure 10 shows the normal stress $\overline{u_3^2}$ which is the fluctuating velocity parallel to the smooth wall. Although, in the case of the ducts with smooth walls, it is limited by the existence of a wall perpendicular to the fluctuating direction and, as a result, the maximum appears near a wall parallel to the fluctuating direction, in this case with the rough walls, the maximum value

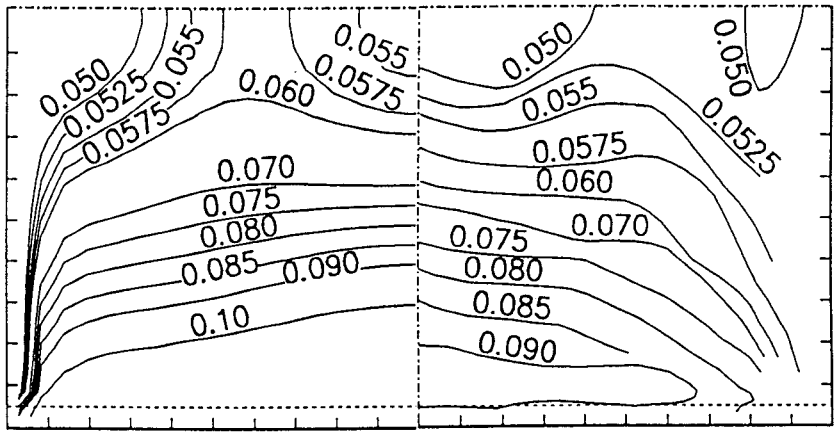

(a) Present calculation (b) Experiment by Fujita *et al.* [2]

Fig.9: Comparison of normal stress $\sqrt{\overline{u_2^2}}/U_s$

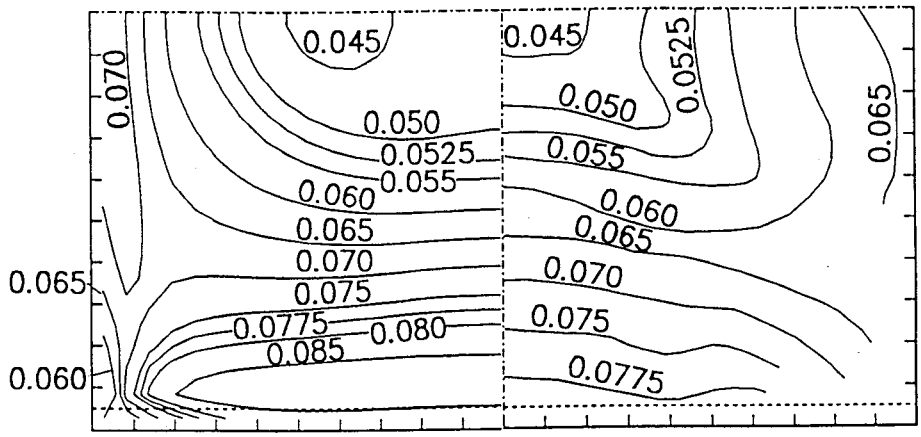

(a) Present calculation (b) Experiment by Fujita *et al.* [2]

Fig.10: Comparison of normal stress $\sqrt{\overline{u_3^2}}/U_s$

of it takes place near the rough wall side. Thus the generation of the normal stress $\overline{u_3^2}$ is caused by the roughness elements, the intensity of the normal stress $\overline{u_2^2}$ indicates larger value than the normal stress $\overline{u_3^2}$.

Figure 11 shows the distribution of the wall shear stress τ_w along the smooth wall obtained by the experiment [2] and the present result, which is nondimensionalized by the averaged value of $\overline{\tau}_w$ along the peripheral wall. It is a characteristic feature in the experimental results that the shear stress decreases as X_3/D_h approaches to zero, that is, to the center of the smooth wall. This is caused by the secondary flow of the second kind, which transfers the low velocity fluid

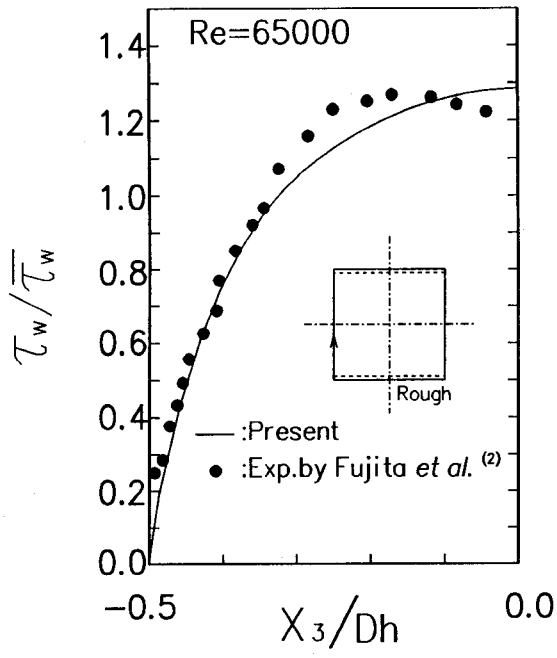

Fig.11: Comparison of wall shear stress

to the region of $X_3/D_h = 0$. The calculated result does not predict accurately this reduction of the wall shear stress. Since it estimates the secondary flow small.

3.3 Examination of Vorticity Balance

The vorticity balance is examined in a square duct flow with roughened wall by evaluating the several terms in the vorticity transport equation using the calculated results for both of the ducts with and without roughened walls, in order to clarify the mechanism for generation of secondary flow. For a steady incompressible constant-property flow, the vorticity transport equation for streamwise vorticity is expressed as follows:

$$\begin{aligned} & U_1\frac{\partial\omega_1}{\partial X_1}+U_2\frac{\partial\omega_1}{\partial X_2}+U_3\frac{\partial\omega_1}{\partial X_3}-\omega_1\frac{\partial U_1}{\partial X_1}-\omega_2\frac{\partial U_1}{\partial X_2}-\omega_3\frac{\partial U_1}{\partial X_3} \\ & =\frac{\partial}{\partial X_1}\left(\frac{\partial\overline{u_1u_2}}{\partial X_3}-\frac{\partial\overline{u_1u_3}}{\partial X_2}\right)+\frac{\partial^2}{\partial X_2\partial X_3}\left(\overline{u_2^2}-\overline{u_3^2}\right) \\ & \quad +\left(\frac{\partial^2}{\partial X_3^2}-\frac{\partial^2}{\partial X_2^2}\right)\overline{u_2u_3}+\nu\left(\frac{\partial^2\omega_1}{\partial X_1^2}+\frac{\partial^2\omega_1}{\partial X_2^2}+\frac{\partial^2\omega_1}{\partial x_3^2}\right) \end{aligned} \tag{16}$$

where the components of the vorticity vector are:

$$\omega_1=\frac{\partial U_3}{\partial X_2}-\frac{\partial U_2}{\partial X_3},\qquad \omega_2=\frac{\partial U_1}{\partial X_3}-\frac{\partial U_3}{\partial X_1},\qquad \omega_3=\frac{\partial U_2}{\partial X_1}-\frac{\partial U_2}{\partial X_2}. \tag{17}$$

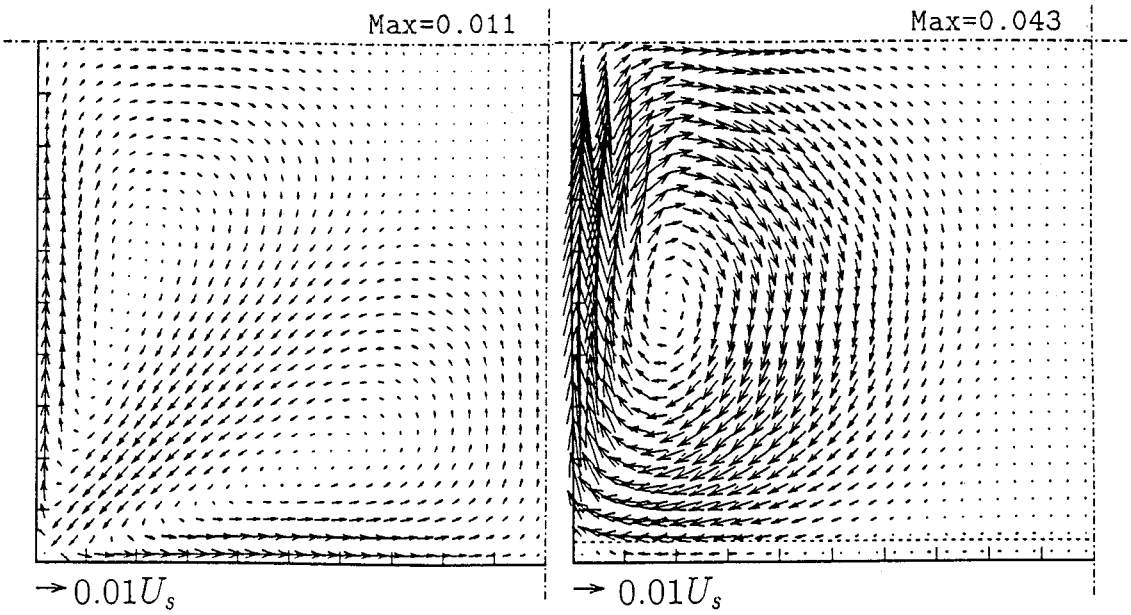

(a) Smooth walls (b) Roughened walls

Fig.12: Velocity vector of the secondary flow

The above equation is rewritten for a fully developed turbulent flow as follows:

$$U_2\frac{\partial\omega_1}{\partial X_2}+U_3\frac{\partial\omega_1}{\partial X_3}=\frac{\partial^2}{\partial X_2\partial X_3}\left(\overline{u_2^2}-\overline{u_3^2}\right)+\left(\frac{\partial^2}{\partial X_3^2}-\frac{\partial^2}{\partial X_2^2}\right)\overline{u_2u_3}$$
$$+\nu\left(\frac{\partial^2\omega_1}{\partial X_2^2}+\frac{\partial^2\omega_1}{\partial X_3^2}\right). \tag{18}$$

The first and second terms of left hand side of (18) represent the convection of the vorticity by the mean flow, and the first and second terms of right hand side of it express the influences of the turbulent stresses on the production or the destruction of the streamwise vorticity, and the third term is the damping by viscosity. The secondary flow of the second kind is caused by anisotropy of the turbulent stresses, namely, by the first and the second terms on the right hand side of (18). The distributions of these production terms are evaluated in two cases of the ducts with and without roughened walls using the calculated results, and compared with those in the duct with smooth walls.

Figure 12(a) and (b) show the velocity vector of the secondary flow of the second kind for both of the smooth wall duct (a) and the roughened walls (b).

Figure 13 shows the nondimensional vorticity in the mean flow direction X_1. In both cases, closed isolines of vorticity is generated by the secondary flow and isolines appeared in near walls are produced by the velocity gradient due to the non-slip condition. In the distribution of Fig.13, the large secondary flow is recognized in near wall of corner region in (a) duct with

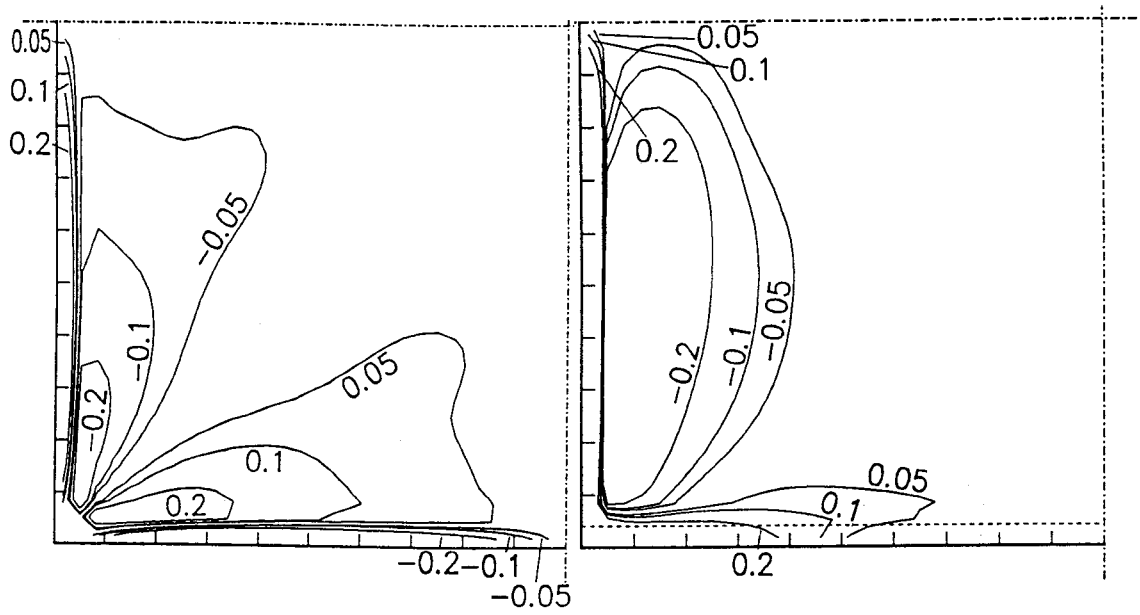

(a) Smooth walls (b) Roughened walls

Fig.13: Contours of vorticity

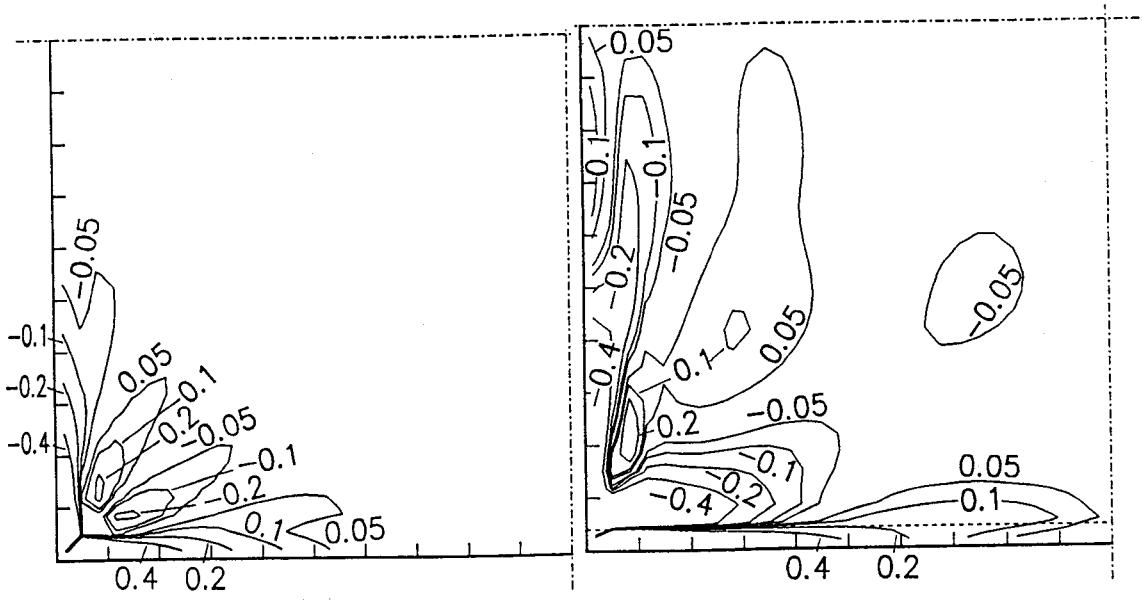

(a) Smooth walls (b) Roughened walls

Fig.14: Contours of production term generated by normal stress

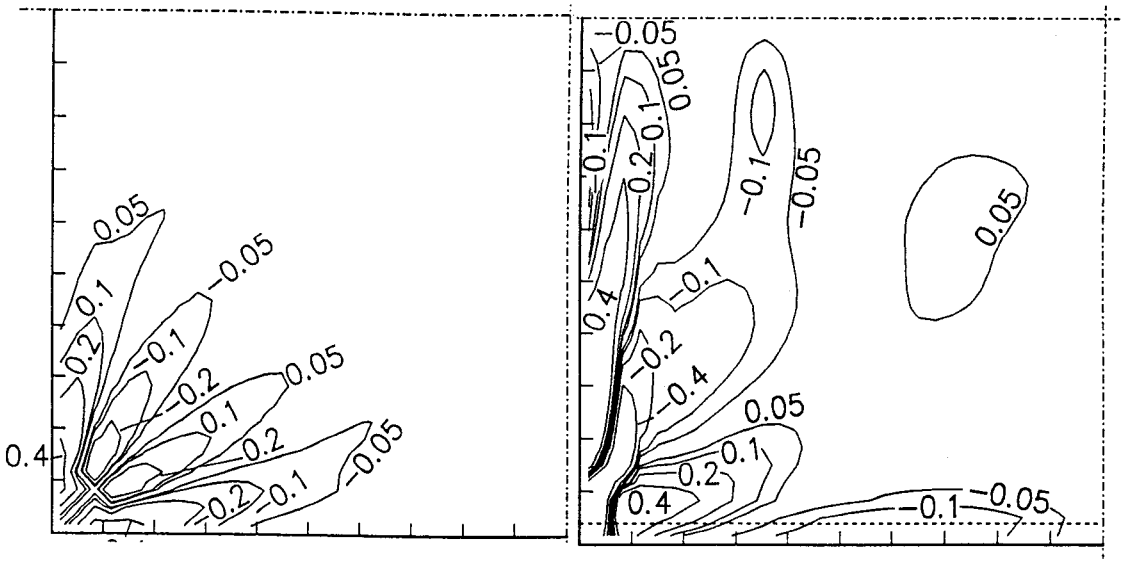

(a) Smooth walls (b) Roughened walls

Fig.15: Contours of production term generated by shear stress

smooth wall. Contrary to that, in a duct with roughened wall (b), the large secondary flow is broadly appears near wall along the smooth wall.

Figures 14 and 15 outline the production terms influenced by the normal stresses and the one of the shear stress, respectively. Brundrett and Baines [17] concluded that the streamwise vorticity was produced by the second derivative of the normal stresses and then convected to the regions where the vorticity is destroyed by the viscous-damping. Demuren and Rodi [7] concluded that the anisotropies of the normal components of the turbulent stress and of the shear component of it have major contributions to the dynamics of the mean flow vorticity. As seen in these figures, the first and second terms of (18) are of the same order with the opposite sign and the distributions of it bear a close resemblance each other regardless with the roughness of the wall surface. Judging from these, the present calculation shows good agreements with the results of [7]. Recently, Kajishima *et al.* [18] and Madabhushi *et al.* [19] pointed out, on the basis of large eddy simulation, that the total production term summed the first and the second terms is almost balanced with the destruction effect of the viscosity near the wall of corner region. From this point of view, the present method can not accurately predict the viscosity effect since the present Reynolds stress model is classified as high Reynolds stress model using wall function.

The large absolute values of the first and second production terms of (18) appears near wall of corner region in the duct with smooth walls. In the duct with roughened walls, the large absolute value of the first term of (18) is observed near both of the smooth and the rough walls of the corner region and the one of the second term of (18) appears near wall along the smooth wall rather than rough wall. Therefore, the secondary flow caused by the anisotropy of the

turbulent stresses is generated near the region with the large production term in the square ducts.

Nextly, in order to find the acting direction of the parameters related to the generation of the secondary flow in the ducts with smooth and roughened walls, each term of the momentum transfer equation is evaluated. The one in the secondary flow direction is given by:

$$U_2\frac{\partial U_j}{\partial X_2}+U_3\frac{\partial U_j}{\partial X_3}=-\frac{1}{\rho}\frac{\partial P}{\partial X_j}-\frac{\partial \overline{u_2u_j}}{\partial X_2}-\frac{\partial \overline{u_ju_3}}{\partial X_3}$$
$$+\nu\left(\frac{\partial^2 U_j}{\partial X_2^2}+\frac{\partial^2 U_j}{\partial X_3^2}\right),\quad j=2,\ 3. \tag{19}$$

Figures 16, 17 and 18 show the vector diagrams of the normal stress gradient, the shear stress gradient and the pressure gradient, respectively. In these figures, calculation results are shown in corner region and H represents the duct width. The left of these figures (a) represents the one with the smooth wall and the right of these figures (b) expresses the result in a duct with roughened wall. The vector of each diagram is defined as follows:

$$\left(-\frac{\partial \overline{u_2^2}}{\partial X_2},\ -\frac{\partial \overline{u_3^2}}{\partial X_3}\right) \tag{20}$$

$$\left(-\frac{\partial \overline{u_2u_3}}{\partial X_3},\ -\frac{\partial \overline{u_2u_3}}{\partial X_2}\right) \tag{21}$$

$$\left(-\frac{\partial P}{\partial X_2},\ -\frac{\partial P}{\partial X_3}\right). \tag{22}$$

As seen in Fig.16, the vectors of the derivatives of the normal stresses point toward the corner in the square duct with smooth wall. Comparing the vectors in the smooth wall duct with ones in the rough wall duct, it is also pointed out that, in rough wall duct, downward vectors toward smooth wall and leftward vectors toward rough wall are observed and values of vector in rough wall duct are greater than it in smooth wall duct. On the other hand, the vectors for derivative of shear stress show complicated behavior. But it is characteristic feature that vector diagram of smooth wall duct is similar to that of rough wall duct. The vectors of pressure gradients, shown in Fig.18, point toward the inner region from the wall at near wall region in both cases. These directions of vectors are opposite direction of the normal stress gradient as shown in Fig.16. This is comprehended as a result of balancing with the normal stress gradient. From these calculated results, it is also interpreted about generation of the secondary flow by using the momentum transport equation that the secondary flow is produced in consequence of the imbalance between the gradient of the turbulent stress and that of the pressure gradient.

4. CONCLUSIONS

A numerical analysis has been performed for fully developed turbulent flow in a square duct with two roughened facing walls by using an algebraic stress model. The calculated results were compared with the experimental data [2]. Moreover, in order to clarify the mechanism of

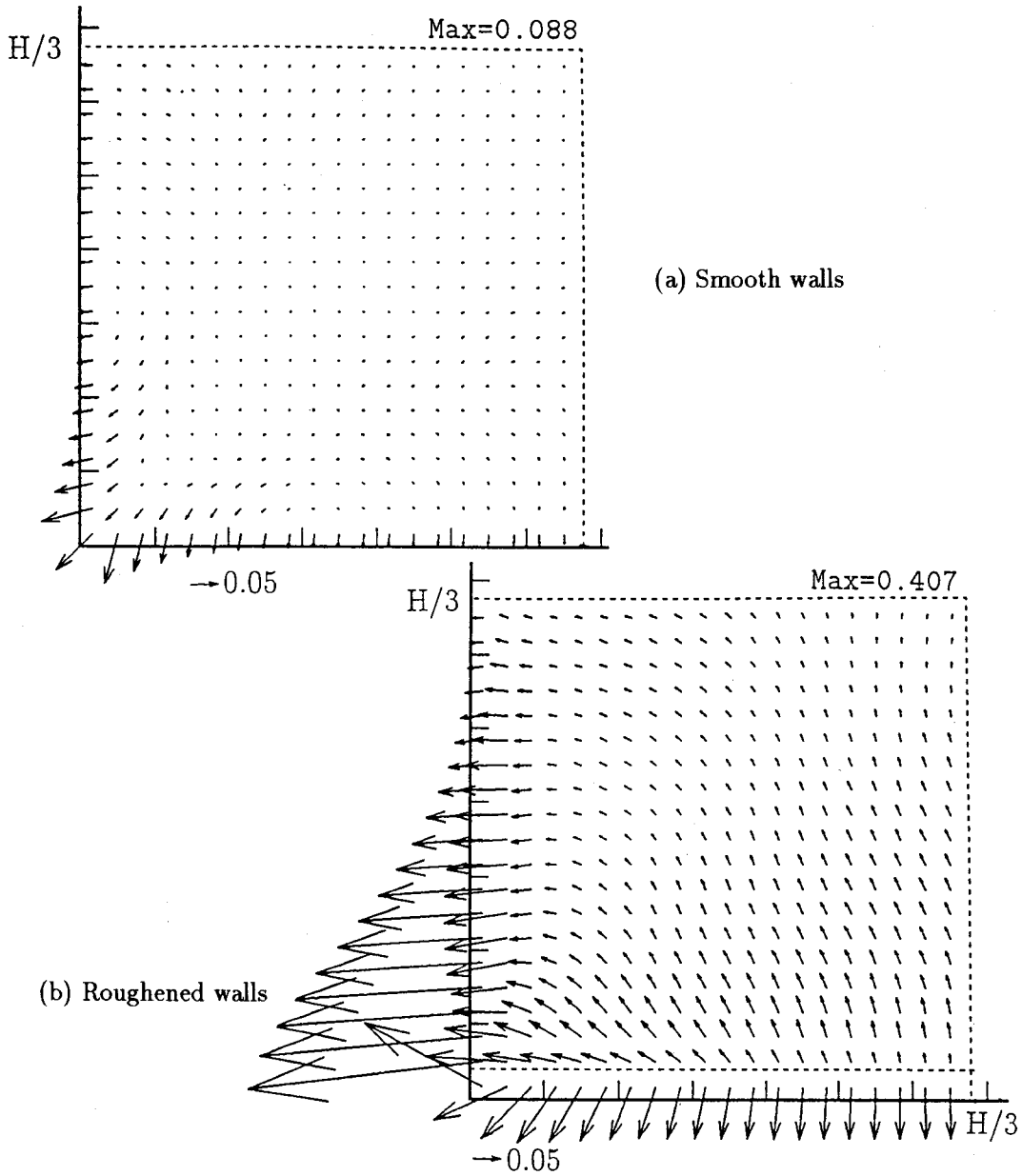

Fig.16: Vector diagram of normal stress gradient $\left(-\frac{\partial \overline{u_2^2}}{\partial X_2}, -\frac{\partial \overline{u_3^2}}{\partial X_3}\right)$

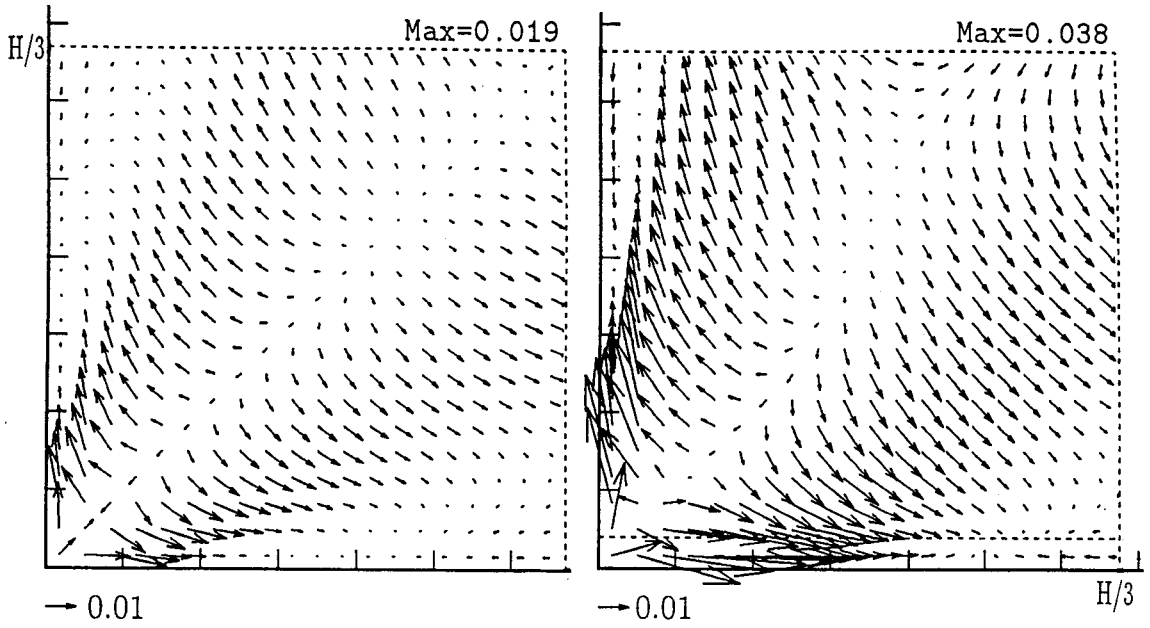

(a) Smooth walls (b) Roughened walls

Fig.17: Vector diagram of shear stress gradient $\left(-\frac{\partial \overline{u_2 u_3}}{\partial X_3}, -\frac{\partial \overline{u_2 u_3}}{\partial X_2}\right)$

production of the secondary flow, vorticity balance is examined by evaluating the production term in the vorticity transport equation using the calculated results in the both cases of the square duct with smooth walls and with two roughened walls. The vector diagrams for the gradient of the turbulent stress and pressure gradient are studied by using the momentum transfer equation.

As a result of this calculation, it is concluded that the present method can predict more accurately the location of the center of secondary flow and the calculated results of the distribution of the normal stresses and turbulent energy are in good agreement with the data of the experiment. From the examination of vorticity balance, it may be said that the distribution of the production term generated by normal stresses is similar to that of shear stress with opposite sign in both duct cases.

Predicting accurately the turbulent flow involved near wall region, it is necessary to adopt the turbulent model for low Reynolds number flow. But, when the turbulent model for near wall is applied to square duct with roughened wall, it is difficult to calculate from the reason why it is necessary to consider the roughness element. From point of this view, the present method, which is characterized to regard the roughness element as boundary condition, is available for engineering fields.

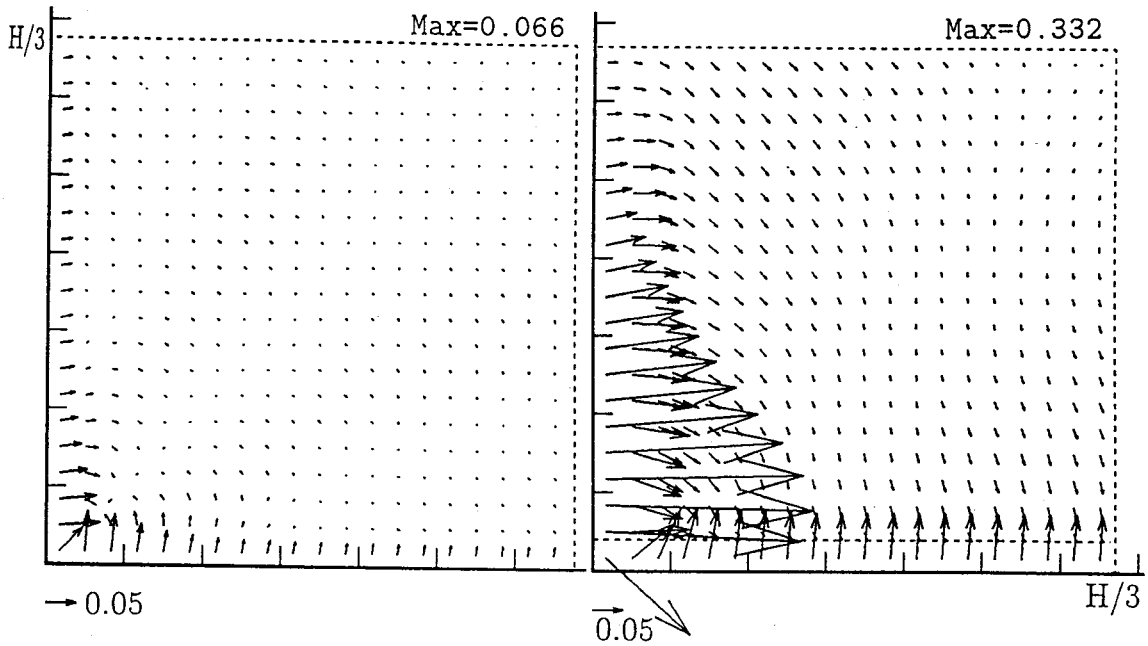

(a) Smooth walls (b) Roughened walls

Fig.18: Vector diagram of pressure gradient $\left(-\frac{1}{\rho}\frac{\partial P}{\partial X_2}, -\frac{1}{\rho}\frac{\partial P}{\partial X_3}\right)$

Acknowledgments

The authors wish to express their appreciation to Prof. H.Fujita, Nagoya University, who kindly allowed us to use his experimental results in this paper and also provide us valuable suggestions and discussions on this numerical analysis.

REFERENCES

[1] B.E.Launder, and W.M.Ying (1972) Secondary flows in ducts of square cross-section; J. Fluid Mech., vol.54 pp.289-295

[2] H.Fujita, H.Yokosawa, S.Iwata, and H.Takahama (1986) Turbulent flow in a square duct with roughened walls on two opposite sides; Trans. Jpn. Soc. Mech. Eng., vol.52 no.482 pp.3491-3497 (in Japanese)

[3] H.Fujita, H.Yokosawa, M.Hirota, and S.Nishigaki (1986) Fully developed turbulent flow in a square duct with a rough wall; Trans. Jpn. Soc. Mech. Eng.,(in Japanese) vol.53 no.492 pp.2370-2376

[4] J.A.C.Humphrey, and J.H.Whitelaw (1980) Turbulent Flow in a duct with roughness; Turbulent Shear Flows 2, pp.174-188

[5] M.Hirota, H.Fujita, H.Yokosawa, S.Kagami, and T.Murofushi; Forced convection heat transfer for turbulent flow in a square duct with a rough wall; Trans. Jpn. Soc. Mech. Eng.,(in Japanese) vol.58 no.548 pp.1200-1208

[6] K.Hanjalic, and B.E.Launder (1972) A Reynolds stress model of turbulence and its

application to thin shear flows; J. Fluid Mech., vol.52 pp.609-638
[7] A.O.Demuren, and W.Rodi (1984) Calculation of turbulent-driven secondary motion in non-circular ducts; J. Fluid. Mech., vol.140 pp.189-222
[8] J.O.Hinze (1973) Experimental investigation of secondary currents in the turbulent flow through a straight conduit; Appl. Sci. Res., vol.28 pp.453-465
[9] H.Fujita, H.Yokosawa, M.Hirota, and C.Nagata (1988) Fully developed turbulent flow and heat transfer in a square duct with two roughened facing walls; Chem. Eng. Comm., vol.74 pp.95-110
[10] B.E.Launder, and W.H.Ying (1973) Prediction of flow and heat transfer in ducts of square cross-section; Heat and Fluid Flow, vol.3 pp.115-121
[11] H.Sugiyama, M.Akiyama, and T.Serizawa (1991) Numerical analysis of developing flow in a square duct using Reynolds stress model; Proc. of the ASME/JSME Thermal Eng. Joint Conf. 1991, vol.3 pp.159-165
[12] W.Rodi (1976) A new algebraic relation for calculating the Reynolds stresses; Z. Angew. Math. Mech., 56 pp.T219-T221
[13] P.Y.Chou (1945) On velocity correlations and the solutions of the equations of turbulent fluctuation; Quart. Appl. Math., vol.3 pp.38-54
[14] B.E.Launder, G.J.Reece, and W.Rodi (1975) Progress in the development of a Reynolds stress turbulence closure; J. Fluid Mech., vol.68 pp.537-566
[15] F.H.Champagne, V.G.Harris, and S.Corrsin (1970) Experiments on nearly homogeneous turbulent shear flow; J. Fluid Mech., vol.41 pp.81-139
[16] V.G.Harris, J.A.H.Graham, and S.Corrsin (1977) Further experiments in nearly homogeneous turbulent shear flow; J. Fluid Mech., vol.81 pp.657-687
[17] E.Brundrett, and W.D.Baines (1964) The production and diffusion of vorticity in duct flow; J. Fluid Mech., vol.19 pp.375-394
[18] T.Kajishima, Y.Miyake, and T.Nishimoto (1991) Large eddy simulation of turbulent flow in a square duct; Trans. Jpn. Soc. Mech. Eng., (in Japanese) vol.57 No.540 pp.2530-2537
[19] R.Madabhushi, and S.P.Vanka (1991) Large eddy simulation of turbulent-driven secondary flow in a square duct; Phys. Fluids A., vol.3 No.11 pp.2734-2745